Marine and Petroleum Geology 77 (2016) 235–246

Contents lists available at ScienceDirect

Marine and Petroleum Geology

journal homepage: www.elsevier.com/locate/marpetgeo

Research paper

Hydrate bearing clayey sediments: Formation and gas production concepts

Jaewon Jang [a, *], J. Carlos Santamarina [b]

[a] School of Sustainable Engineering and the Built Environment, Arizona State University, USA
[b] Earth Science and Engineering, King Abdullah University of Science and Technology, Saudi Arabia

ARTICLE INFO

Article history:
Received 30 November 2015
Received in revised form
29 April 2016
Accepted 16 June 2016
Available online 20 June 2016

Keywords:
Gas hydrate
Hydrate lenses
Clayey sediments
Frozen ground

ABSTRACT

Hydro-thermo-chemo and mechanically coupled processes determine hydrate morphology and control gas production from hydrate-bearing sediments. Force balance, together with mass and energy conservation analyses anchored in published data provide robust asymptotic solutions that reflect governing processes in hydrate systems. Results demonstrate that hydrate segregation in clayey sediments results in a two-material system whereby hydrate lenses are surrounded by hydrate-free water-saturated clay. Hydrate saturation can reach ≈2% by concentrating the excess dissolved gas in the pore water and ≈20% from metabolizable carbon. Higher hydrate saturations are often found in natural sediments and imply methane transport by advection or diffusion processes. Hydrate dissociation is a strongly endothermic event; the available latent heat in a reservoir can sustain significant hydrate dissociation without triggering ice formation during depressurization. The volume of hydrate expands 2-to-4 times upon dissociation or CO_2–CH_4 replacement. Volume expansion can be controlled to maintain lenses open and to create new open mode discontinuities that favor gas recovery. Pore size is the most critical sediment parameter for hydrate formation and gas recovery and is controlled by the smallest grains in a sediment. Therefore any characterization must carefully consider the amount of fines and their associated mineralogy.

1. Introduction

Fine-grained sediments host more than 90% of the accumulated global gas hydrate [Boswell 2009; Boswell and Collett 2011]. Well known accumulations of hydrate-bearing clayey sediments include those in the Gulf of Mexico, Krishna-Godavari basin, Blake Ridge, Cascadia Margin, Ulleung Basin, and Hydrate Ridge [Dai et al., 2011]. Hydrates in all these cases are found as segregated masses forming features such as lenses and nodules.

Hydro-thermo-chemo-mechanically coupled processes that occur during hydrate formation and dissociation affect the spatial distribution of hydrate in sediments and also control gas production during depressurization, heating and CO_2–CH_4 replacement.

Hydrate formation and dissociation in clayey sediments is strongly affected by pore size. The sediment porosity n decreases with sediment depth due to self compaction. In terms of void ratio $e = n/(1\text{-}n)$, the sedimentation compression curve can be expressed as a function of the overburden effective stress σ` [Burland 1990; Skempton 1969; Terzaghi and Peck 1948]:

$$e = e_{100} - C_C log\left(\frac{\sigma'}{100kPa}\right) \quad (1)$$

where e_{100} is the void ratio at $\sigma` = 100$ kPa and $C_C$ is the sediment compressibility. The two constitutive parameters $e_{100}$ and $C_C$ increase with the sediment specific surface $S_S$ [$m^2$/g]. However, the change in vertical effective stress dσ` between depths z and $z + dz$ depends on the sediments saturated unit weight $\gamma_s = \gamma_w (G_s + e)/(1 + e)$

$$d\sigma` = (\gamma_s - \gamma_w)dz = \gamma_w \frac{(G_s - 1)}{(1 + e)} dz \quad (2)$$

where γ_w is the unit weight of water and G_s is the specific gravity of minerals that make the grains. Equations 1&2 are combined and integrated with depth to compute the depth varying overburden effective stress and void ratio (hence, porosity).

* Corresponding author.
E-mail addresses: jjang19@asu.edu (J. Jang), Carlos.santamarina@kaust.edu.sa (J.C. Santamarina).

http://dx.doi.org/10.1016/j.marpetgeo.2016.06.013
0264-8172/

Notation

α	metabolizable carbon content
α_g	ratio of $\rho_g c_g$ to $\rho_w c_w$, $\alpha_g = \rho_g c_g/\rho_w c_w$
α_h	ratio of $\rho_h c_h$ to $\rho_w c_w$, $\alpha_h = \rho_h c_h/\rho_w c_w$
α_m	ratio of $\rho_m c_m$ to $\rho_w c_w$, $\alpha_m = \rho_m c_m/\rho_w c_w$
β	ratio of carbon molecular mass to methane molecular mass
β_h	ratio of $\rho_h L_h$ to $\rho_w c_w$, $\beta_h = \rho_h L_h/\rho_w c_w$
β_I	ratio of $\rho_w L_I$ to $\rho_w c_w$, $\beta_h = L_l/c_w$
δ	thickness of hydrate lens
η	fluid volume expansion after hydrate dissociation
θ	contact angle
κ	volume fraction of segregated hydrate
λ	mole of methane per unit volume of hydrate
$\rho_{CH4\text{-}G}$	methane gas density
$\rho_{CO2\text{-}G}$	gaseous carbon dioxide density
$\rho_{CO2\text{-}L}$	liquid carbon dioxide density
ρ_g	gas density
ρ_h	hydrate density
ρ_m	mineral density
ρ_w	water density
ρ_{w_hyd}	water mass in unit volume of hydrate
$\sigma`$	effective stress
φ	fraction of fines in sediment
χ	hydration number (e.g., $CH_4 \cdot \chi H_2O$ or $CO_2 \cdot \chi H_2O$)
ω	compressibility factor
γ_{hw}	interfacial tension between hydrate and water
γ_s	sediment unit weight
γ_w	water unit weight
c_g	specific heat of gas
c_h	specific heat of hydrate
c_m	specific heat of mineral
c_w	specific heat of water
C_A	solubility of methane in water after hydrate formation
C_B	solubility of methane in water before hydrate formation
C_C	sediment compressibility
C_H	methane concentration per kg of hydrate
d_{pore}	pore diameter
e	void ratio
e_c	void ratio of coarse particles
e_f	void ratio of fine particles
e_{100}	void ratio at $\sigma` = 100$ kPa
E_{DIS}	energy needed to dissociate hydrate
E_{HBS}	sensible energy available in sediment before hydrate dissociation
FR_{WI}	fraction of ice formed during hydrate dissociation
G_s	specific gravity of minerals
ΔH	enthalpy
k_H^o	Henry's constant
m_h	molecular weight of gas hydrate
L	lens-to-lens spacing
L_H	transformation heat of hydrate
L_I	transformation heat of ice
M_C	mass of metabolizable carbon
M_{CH4}	methane mass
M_F	mass of fine particles
M_H	hydrate mass
M_M	mineral mass
$M_{P,T}$	gas concentration in water under pressure P and temperature T condition
M_T	mass of sediment composed of coarse and fine particles
n	porosity
n_0	initial porosity of sediment before hydrate formation
n_f	final porosity of sediment after hydrate segregation
$n_{CH4\text{-}H}$	mole of methane in CH_4 hydrate
P	pressure
P_C	capillary pressure
P_H	pressure inside hydrate
P_F	final pressure after hydrate dissociation
P_0	initial pressure before hydrate dissociation
P_W	water pressure
R	universal gas constant
S_H	hydrate saturation
S_s	specific surface
S_w	water saturation
T_{Bulk}	hydrate formation/dissociation temperature in bulk water
T	temperature
T_o	initial temperature before hydrate dissociation
T_F	final temperature after hydrate dissociation
T_T	temperature of hydrate phase boundary
ΔT_{dep}	hydrate formation/dissociation temperature depression in small pores
ΔT_{HW}	temperature change of water by the energy equivalent to dissociate the same mass of hydrate
ΔT_{IW}	temperature change of water by the energy equivalent to melt the same mass of ice
$V_{CH4\text{-}G}$	volume of CH_4 gas
$V_{CH4\text{-}H}$	volume of CH_4 hydrate
$V_{CO2\text{-}H}$	volume of CO_2 hydrate
$V_{CO2\text{-}L}$	volume of liquid CO_2
V_G	gas volume
V_H	hydrate volume
V_T	total sediment volume
V_V	volume of voids
V_W	water volume
z	depth

The mean pore size d_{pore} can be estimated from the void ratio e, specific surface S_s [m^2/g] and the mineral mass density ρ_m:

$$d_{pore} = \frac{4e}{S_s \rho_m} \tag{3}$$

For reference, the mean pore size for kaolinite 1 m below the seafloor, $z = 1$ mbsf, is $d_{pore} \approx 200$ nm ($e_{100} = 1.04$, $C_c = 0.35$, $S_s = 10$ m^2/g), while the mean pore size for bentonite at $z = 1000$ mbsf is $d_{pore} \approx 5$ nm ($e_{100} = 3.2$, $C_c = 1.2$, $S_s = 300$ m^2/g). Small pore size in clayey sediments affects gas solubility, the phase boundary, hydrate morphology and the properties of the hydrate bearing sediments.

The purpose of this study is to review the fundamental concepts relevant to hydrate formation in clayey sediments and to explore potential phenomena pertinent to gas production. We analyze coupled pore-scale phenomena and present simple yet robust asymptotic expressions to obtain order-of-magnitude estimates that can aid in the understanding of hydrate bearing clayey sediments and guide the design of gas production strategies. The

replacement of CH_4 with CO_2 is a possible production alternative; hence, parameters relevant to CO_2 solubility and phase boundaries are reported in parallel to parameters for CH_4.

2. Phase boundary and gas solubility

Pressure and temperature affect the composition of the hydrate mass. The CH_4 molecule is smaller than CO_2 and fits more easily into the two small cages in Structure I hydrate. Thus, the stoichiometric ratio for CH_4 hydrate ($\chi = 5.8$-to-6.0) is closer to the theoretical value $\chi = 46/8 = 5.75$ and is less sensitive to pressure than the stoichiometric ratio of CO_2 hydrate (χ~6.6 at 1.3 MPa and decreases to $\chi < 6$ at 4.5 MPa) [Anderson et al., 2003; Circone et al., 2003; Jung et al., 2010; Klapproth et al., 2003]. More importantly, pressure and temperature define the stability field and gas solubility. The role of small pores in fine grained sediments and competing solutes on the phase boundary and gas solubility are reviewed next in relation to hydrate formation in clayey sediments.

2.1. Phase boundary

The hydrate phase boundary is affected by several factors that alter molecular activity, e,g, the interaction with mineral surfaces and the presence of other ions and molecules, including salts and mixed gases.

Pore size effects. Small hydrate nuclei are in equilibrium with the pore fluid at higher gas concentrations than the concentration around larger hydrate crystals, known as the Gibbs-Thomson effect. Therefore, hydrate experiences formation/dissociation (or phase transformation) and temperature depression ΔT_{dep} for small pores sizes d_{pore} [Anderson et al., 2003; Kwon et al., 2008],

$$\Delta T_{dep} = -\frac{4}{d_{pore}}\left(\frac{\gamma_{hw} m_h \cos\theta}{\rho_h L_H}\right) T_{bulk} \quad (4)$$

where the variables are the hydrate-water interfacial tension γ_{hw} [N/m], the molecular weight of gas hydrate m_h [g/mol], the contact angle θ, the hydrate mass density ρ_h [kg/m^3], the heat of hydrate dissociation L_H [kJ/kg], and hydrate formation/dissociation temperature in bulk water T_{Bulk} [K]. Tables 1 and 2 summarize typical values for these parameters.

Fig. 1a&b present a compilation of measured temperatures during CH_4 and CO_2 hydrate formation/dissociation. The phase boundaries for hydrate in bulk water are obtained from experimentally validated thermodynamic models [Duan and Sun 2003; Jung et al., 2010; Sun and Duan 2005]. Trends predicted by the Gibbs-Thomson equation (Equation (4)) are superimposed on the figure. We can conclude that pore size effects vanish when pores are larger than d_{pore}~100 nm. The Gibbs-Thompson equation combines with the effective stress dependent pore size (Equation (1)-through-4) to anticipate deviations in the stability field in deep clayey sediments [Dai et al., 2011; Henry et al., 1999].

Salinity effects. The Coulombic attraction between water molecules and ions is stronger than the attraction between the water molecules and the guest molecule in gas hydrate. Therefore, substantial sub-cooling is required to cause hydrate to form in salt water [Dickens and Quinby-Hunt 1997; Sloan and Koh 2008].

Mixed gases. The phase boundary for hydrate made from mixed methane and carbon dioxide lies between the boundaries for pure CH_4 and CO_2 hydrates. The relative position scales with the mixture ratio as shown in Fig. 2 [Adisasmito et al., 1991; Seo and Lee 2001]. The CO_2 hydrate boundary shifts to higher pressures even with small amounts of CH_4 [Donnelly and Katz 1954; Sloan and Koh 2008]. Note that the stability of CH_4 hydrate requires higher pressures than CO_2 hydrate for temperatures $T \leq 283.67$ K. However, this is not the case at higher temperatures. In-situ methane hydrate bearing sediments are typically encountered under Pressure-Temperature (PT) conditions such that (1) CO_2 injection will be in the liquid phase and (2) any free water would usually form CO_2 hydrate (gas-limited reservoirs). This situation is revisited later in the context of gas production from hydrate bearing clayey sediments.

2.2. Gas solubility

Gas solubility in water in the absence of hydrates. The pressure and temperature PT dependent gas concentration in water $M_{P,T}$ [mol/m^3] can be approximated using Henry's law as a linear function of pressure P:

$$M_{P,T} = P k_H^0 \cdot \exp\left[\frac{-\Delta H}{R}\left(\frac{1}{T} - \frac{1}{298.15\text{K}}\right)\right] \times \quad \text{in bulk and without hydrates} \quad (5)$$

where k_H^0 is Henry's constant, T is temperature, ΔH is the enthalpy of the solution, and the universal gas constant is $R = 8.314$ J/(mol·K). Typical values for CH_4 in water are $\Delta H = -14130$ J/mol and $k_H^0 = 1.3 \times 10^{-3}$ M/atm at 298.15 K. These parameters for CO_2 in water are $\Delta H = -19940$ J/mol and $k_H^0 = 3.4 \times 10^{-2}$ M/atm at 298.15 K [Osegovic et al., 2006; Wilhelm et al., 1977]. Hence, the solubility of CH_4 and CO_2 in water rises with increasing pressure and decreasing temperature.

Gas solubility in the presence of hydrates. The presence of hydrates stimulates the formation of additional hydrates. Hence the presence of hydrates results in a decrease in the equilibrium concentration of gas in water. In fact, gas solubility trends within the hydrate stability field and in the presence of hydrates are the opposite to trends outside the stability field. Therefore lower temperatures or higher pressures prompt additional hydrate formation and reduces the gas concentration in water [Lu et al., 2008; Waite et al., 2009].

Pore size effects. Gas solubility in water increases with decreasing pore size due to the lower water activity in small pores [Henry et al., 1999; Sun and Duan 2007].

Competing solutes. Hydrated ions reduce the average mobility of water molecules. Therefore, the solubility of gas in water decreases inversely proportional to salt concentration [Davie et al.,

Table 1
Interfacial tension and contact angle.

	Interfacial tension [mN/m]	Contact angle [°]
Water-CH_4 (g)	72[a] (P = 0.1 MPa, T = 298 K) 64[a] (P = 10 MPa, T = 298 K)	105[b] on PTFE (P = 0.1 MPa, T = 298 K)
Water-CH_4 (h)	32[c] 17[d] 39[e]	no available data
Water-CO_2 (g)	72[b] (P = 0.1 MPa, T = 298 K)	~38[b] on calcite (P > 7 MPa, 298 K)
Water-CO_2 (l)	30[b] (P = 7 MPa, T = 298 K)	~30[b] on calcite (P>~7 MPa, T = 298 K) ~20[b] on quartz (P<~7 MPa, T = 298 K)
Water-CO_2 (h)	30[c] 14[d]	no available data

[a] Ren et al. (2000).
[b] Espinoza and Santamarina (2010).
[c] Anderson et al. (2003).
[d] Uchida et al. (2002).
[e] Uchida et al. (1999).

Table 2
Physical properties of water, ice, mineral, methane, carbon dioxide, and methane and carbon dioxide hydrate.

	Specific heat [kJ/(kg °C)]	Heat of transformation [kJ/kg]	Density [kg/m^3]
Water	4.218 (273 K)[a] 4.192 (283 K)[a] 4.2174 (273 K)[c]	For water mass, 334.2 (273.2 K)[b] 336 (273.1 K)[c]	999.9 (273 K)[a] 999.7 (283 K)[a]
Ice	2.014 (260 K)[b] 1.957 (260 K)[c] 2.097 (270 K)[b] 2.052 (270 K)[c] 2.097 (273 K)[d]	–	917 (273 K)[e]
Quartz	0.73 (273 K)[d] 0.71 (273 K)[f] 0.8 (286–373 K)[f]	–	2650[g] 2620[f]
CH_4 (g)	2.26 (298 K, 0.1 MPa)[f] 2.259 (280 K, 1 MPa)[g] 3.813 (280 K, 20 MPa)[g]	2290 (Heat of combustion)[f]	7.04 (280 K, 1 MPa)[g] 177.56 (280 K, 20 MPa)[g]
CO_2 (g)	0.819 (275 K)[f] 2.47 (273 K)[f]	–	983[f] (273 K, 3.4 MPa)
CO_2 (l)	2.5694 (274 K 3.5642 MPa)[h] 2.8141 (280 K, 4.1607 MPa)[h] 2.2798 (280 K, 10 MPa) [h]]	–	922.3 (274 K 3.5642 MPa)[h] 883.58 (280 K, 4.1607 MPa)[h] 938.22 (280 K, 10 MPa)[h]
CH_4 hydrate	2.003 (260 K for $CH_4 \cdot 6H_2O$)[i] 2.077 (270 K for $CH_4 \cdot 6H_2O$)[i] 0.0061 (T-273) + 2.16 (274–290 K, 31.5 MPa)[j] 0.0033 ·(T-273) + 2.14 (287.4 K, 31.5–102 MPa)[j]	For $CH_4 \cdot \chi H_2O$ 437.1[i] 430.3 (283.15 K, $\chi = 5.98$)[k] 470.4 (278.15 K, $\chi = 5.97$)[k] 429.8[l] 434.4 (273.65 K, $\chi = 6.38$)[m]	922 (283 K, 5 MPa)[j] 910[r&s]
CO_2 hydrate	No data found	For $CO_2 \cdot \chi H_2O$ 374.5 (273.65 K, $\chi = 7.23$)[m] 390.7–398.5 (at quadruple points, $\chi = 6.6$–5.6)[n]	1065[o] 1054[p] 1090–1110[q]

[a] Weast (1987).
[b] Handa et al. (1984).
[c] Leaist et al. (1982).
[d] Kaye and Laby (2007).
[e] Dvorkin et al. (2000).
[f] Engineering ToolBox (www.engineeringtoolbox.com).
[g] Sychev et al. (1987).
[h] Span and Wagner (1996).
[i] Handa (1986).
[j] Helgerud et al. (2009).
[k] Lievois et al. (1990).
[l] Rueff et al. (1988).
[m] Kang et al. (2001).
[n] Anderson (2003).
[o] Anderson et al. (2003).
[p] Uchida et al. (2002).
[q] Aya et al. (1997).
[r] Kiefte et al. (1985).
[s] Sloan and Koh (2008).

2004; Sun and Duan 2007; Tishchenko et al., 2005; Zatsepina and Buffett 1998]. Likewise, coexisting gases compete for available cavities between water molecules and restrict each others solubilities [Qin et al., 2008].

Summary: General Trends. Published solubility data and additional values computed with solubility calculators can be summarized as follows [Donnelly and Katz 1954; Duan and Sun 2003; Duan and Mao 2006; Folas et al., 2007; Hashemi et al., 2006; Henry et al., 1999; Jung et al., 2010; Servio and Englezos 2001, 2002; Sun and Duan 2007]:

- Before hydrate formation, the solubility of CH_4 in water is C_B~0.08-to-0.20 mol/kg (for *PT* conditions $P < 25$ MPa and $T < 15$ °C). The solubility of CO_2 in water is an order of magnitude higher than that of CH_4 for the same *PT* conditions.
- By comparison, the methane concentration per kg of hydrate is $C_H = 8.06$ mol/kg, that is 40-to-100 times higher than the concentration in water.
- The solubility of gas in water after hydrate formation is approximately half of the solubility of gas in water in the absence of hydrate, for *PT* conditions common to seafloor hydrate accumulations of interest.
- Methane solubility in seawater is approximately ~0.93 ± 0.03 of the methane solubility in fresh water. This ratio is similar in the presence or absence of hydrates.
- Methane solubility in 10 nm small pores can be 1.2 times higher than the solubility of methane in bulk water (Sun and Duan, 2007. Note: Henry et al., 1999 used less accurate factors and obtained an even higher solubility in small pores).

It follows from the these observations that the pore fluid in clayey sediments can sustain a gas saturation 2-to-2.5 times higher before hydrate is formed than after hydrate formation occurs.

3. Hydrate formation in clayey sediments

3.1. Morphology

Force equilibrium requires that the capillary pressure inside hydrate lenses $P_C = P_H - P_W = 4\gamma_{hw}\cos\theta/d_{pore}$ balances the pressure

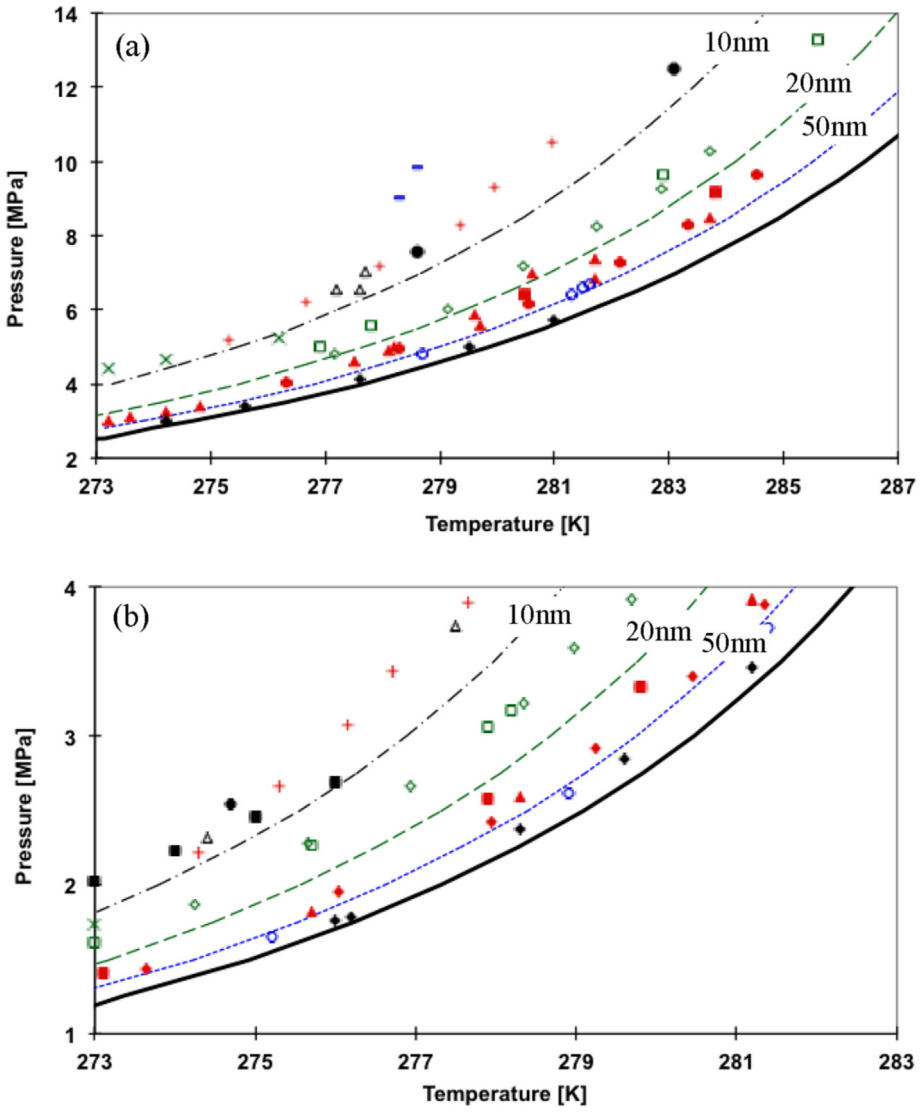

Fig. 1. Hydrate stability in small pores. (a) CH_4 hydrate stability. Theoretical stability boundary of CH_4 hydrates in (black continuous line) bulk phase and (blue dotted line) 50 nm, (green broken line) 20 nm, (black chain line) 10 nm pores. Experimentally obtained stability condition of CH_4 hydrate in (◆) 102.6 nm [Uchida et al., 2002] (○), 49.5 nm [Uchida et al., 2002] (▲), 30.9 nm [Uchida et al., 2002] (●), 30 nm [Seo et al., 2002] (■), 30.6 nm [Anderson et al., 2003] (×), 14 nm [Handa and Stupin, 1992] (◊), 15 nm [Seo et al., 2002] (□), 15.8 nm [Anderson et al., 2003], (Δ) 11.9 nm [Uchida et al., 2002], (●) 9.2 nm [Anderson et al., 2003] (▬), 6 nm [Uchida et al., 2002] (——), 6 nm [Smith et al., 2002a], and (+) 6 nm [Seo et al., 2002] pores. Parameters for Gibbs-Thompson equation are $T_s = 32$ mN/m, $m_h = 119.5$ g/mol, $\cos\theta = 1$, $\rho_{CH4} = 914$ kg/m^3, and $L_f = 53.2$ kJ/mol [Anderson et al., 2003]. (b) CO_2 hydrate stability. Theoretical stability boundary of CO_2 hydrates in (black continuous line) bulk phase and (blue dotted line) 50 nm, (green broken line) 20 nm, (black chain line) 10 nm pores. Experimentally obtained stability condition of CO_2 hydrate in (◆) 102.6 nm [Uchida et al., 2002] (○), 49.5 nm [Uchida et al., 2002] (▲), 30.9 nm [Uchida et al., 2002] (●), 30 nm [Seo et al., 2002] (■), 30.6 nm [Anderson et al., 2003] (×), 15 nm [Smith et al., 2002b] (◊), 15 nm [Seo et al., 2002] (□), 15.8 nm [Anderson et al., 2003], (Δ) 11.9 nm [Uchida et al., 2002], (■) 10 nm [Smith et al., 2002b], (●) 9.2 nm [Anderson et al., 2003], and (+) 6 nm [Seo et al., 2002] pores. Parameters for Gibbs-Thompson equation are $T_s = 30$ mN/m, $m_h = 147.5$ g/mol, $\cos\theta = 1$, $\rho_{CO2} = 1065$ kg/m^3, and $L_f = 65.2$ kJ/mol [Anderson et al., 2003]. (For interpretation of the references to colour in this figure legend, the reader is referred to the web version of this article.)

in the water p_w and the effective stress acting on the grain skeleton σ' [Clennell et al., 1999; Santamarina and Jang 2010]

$$\sigma' = \frac{4\gamma_{hw}\cos\theta}{d_{pore}} \quad \text{condition for hydrate lens} \tag{6}$$

where d_{pore} is the pore diameter in the sediment, the contact angle can be assumed to be $\theta = 0°$ and the hydrate-water interfacial tension is $\gamma_{hw} = 0.035$ N/m [Uchida et al., 1999]. Equation (6) combines with Equation (3) and the integral form of Equation (2) to predict that hydrate will displace grains, segregate and form hydrate lenses or nodules in the upper 0.5 m depth in silt sediments, to a depth of 1500 m in kaolinite, and much deeper in illite and montmorillonite (see compilation of field data in Dai et al., (2012)). Consequently, hydrate bearing clayey sediments are two-material systems made of segregated hydrate lenses or nodules that are surrounded by hydrate-free water-saturated clay. Effective media properties must be evaluated accordingly.

3.2. Hydrate volume fraction from initial excess gas (at constant mass)

Hydrate lenses may form in the absence of advection or diffusion (i.e., in a closed system). This occurs by concentrating the "excess gas" between the solubility of gas in water in the absence of hydrate (enhanced in small pores) and the lower solubility of gas in

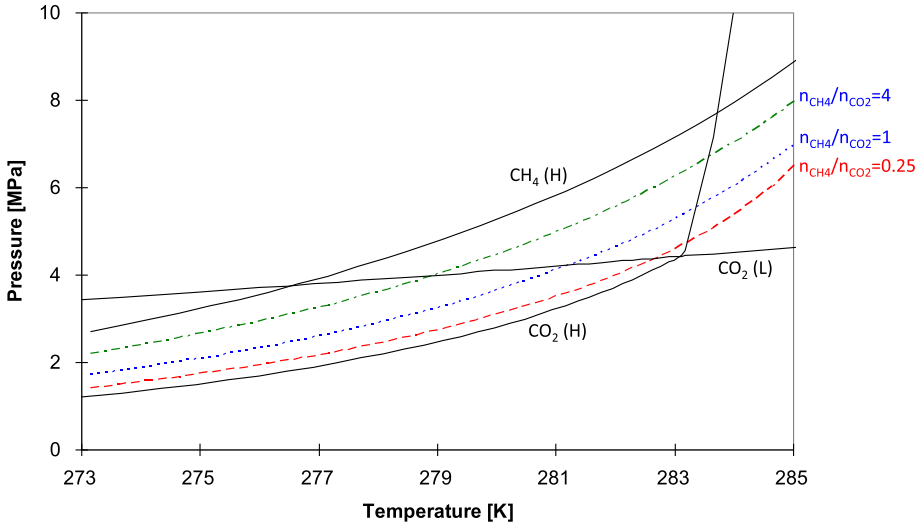

Fig. 2. Hydrate phase boundary – different methane and carbon dioxide gas mixtures. Molar fractions of methane n_{CH4} and carbon dioxide n_{CO2}: (red broken line) $n_{CH4}/n_{CO2} = 0.25$, (blue dotted line) $n_{CH4}/n_{CO2} = 1$, (green chain line) $n_{CH4}/n_{CO2} = 4$. Boundaries are calculated using HydraFLASH [from HYDRAFACT v2.2]. The Liquid-Vapor (L–V) boundary is estimated using the equation developed by Jung et al., (2010). (For interpretation of the references to colour in this figure legend, the reader is referred to the web version of this article.)

water after hydrate formation. Consider a water-saturated clayey sediment at an initial porosity n_o and gas concentration C_B before hydrate formation. After hydrate formation, the concentration of gas in water drops to C_A and the surrounding sediments compact to the final porosity n_f as a result of cryosuction (Fig. 3). Mass conservation equations for water, gas and mineral species combine to predict the volume fraction of segregated hydrate κ and the final porosity n_f of the surrounding clay mass:

$$\kappa = \frac{V_H}{V_T} = \frac{C_B - C_A}{C_H - C_A} n_0 \approx \frac{C_B - C_A}{C_H} n_0 \quad \text{hydrate volume fraction} \tag{7}$$

$$n_f = \frac{n_0 - \kappa}{1 - \kappa} \tag{8}$$

where C_H is the gas concentration in hydrate. In relation to hydrate saturation S_H,

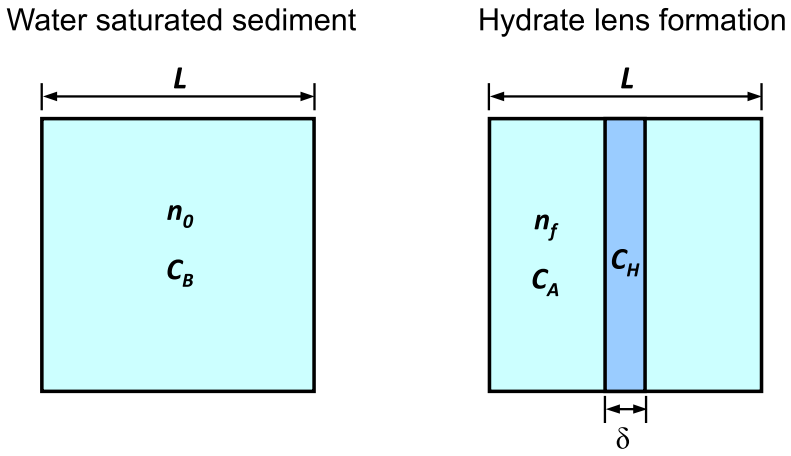

	Before hydrate lens formation		After Hydrate lens formation
Water	$\rho_w L n_0$	=	$\rho_w (L-\delta) n_f + \rho_{w\_hyd}\delta$
Methane	$C_B L n_0$	=	$C_A (L-\delta) n_f + C_H \delta$
Mineral	$\rho_m L (1-n_0)$	=	$\rho_m (L-\delta)(1-n_f)$

Fig. 3. Anticipated hydrate lens thickness that could form from the initially dissolved excess gas. Hydrate lens thickness δ in a medium with lens-to-lens spacing L is a function of the initial porosity n_0, gas solubility in the absence and in the presence of gas hydrate C_B and C_A, and gas concentration in hydrate C_H.

$$S_H = \frac{V_H}{V_T} = \frac{\kappa}{n_0} \approx \frac{C_B - C_A}{C_H} \quad \text{hydrate saturation} \tag{9}$$

For example, consider two clayey sediments under a pore fluid pressure of 20 MPa. The first case is a kaolinite sediment at 50 mbsf with an initial porosity $n_o = 0.45$ and mean pore size $d_{pore} = 120$ nm. The gas concentration before hydrate formation is $C_B \approx 0.18$ mol/kg; under closed conditions, this sediment can develop an initial volume fraction of segregated hydrate $\kappa = 0.6\%$ which corresponds to a hydrate saturation $S_H = 1.4\%$. The surrounding sediment will experience a minor densification from $n_o = 0.45$ to $n_f = 0.447$.

The second case is a montmorillonitic deposit at 250 mbsf, with $n_o = 0.66$ and $d_{pore} = 10$ nm. Under these conditions, it can accumulate 1.5 times higher gas concentration before hydrate formation, $C_B = 1.5C_A$, and it can form an initial volume fraction of segregated hydrate $\kappa = 1.7\%$ or $S_H = 2.2\%$. The surrounding sediment would compact from an initial porosity $n_o = 0.660$ to a final porosity $n_f = 0.655$.

These two end member clayey sediments (within *PT* ranges of interest) allow us to conclude that the volume fraction or saturation of segregated hydrate in lenses or nodules could reach $S_H \approx 1.4\%$–2.2% only when the excess dissolved gas is used in hydrate formation.

3.3. Hydrate volume fraction from available organic carbon (at constant mass)

Hydrate may also form using methane produced by organic mass trapped in the sediment. The sediment in this case is both the source deposit and the reservoir. The maximum amount of hydrate that can form is a function of (1) the initial "metabolizable" carbon content $\alpha = M_C/M_M$, where M_M is the mineral mass and M_C is metabolizable carbon mass, and (2) the ratio $\beta = M_{CH4}/M_C$ between the generated methane mass M_{CH4} and the original mass of metabolizable carbon M_C, i.e., the ratio of their molar masses $\beta = 16/12$ (see detailed discussion in Malinverno (2010), and earlier analyses by Paull et al., [1994], Davie and Buffett [2001], Bhatnagar et al., [2007]). Then, the attainable hydrate saturation is:

$$\begin{aligned} S_H = \frac{V_H}{V_V} &= \frac{M_H}{\rho_h V_V} = \frac{\frac{120}{16} M_{CH4}}{\rho_h V_V} = \frac{\frac{120}{16}\alpha\cdot\beta\cdot M_M}{\rho_h V_V} \\ &= \frac{120}{16}\alpha\cdot\beta\cdot\frac{1-n_0}{n_0}\frac{\rho_m}{\rho_h} \\ &= 10\alpha\frac{1-n_0}{n_0}\frac{\rho_m}{\rho_h} \approx 28\alpha\frac{1-n_0}{n_0} \end{aligned} \tag{10}$$

where the ratio between the mineral and hydrate mass densities is $\rho_m/\rho_h \approx 2.8$. From Equations (7) and (9), the volume fraction of segregated hydrate κ is obtained from the hydrate saturation and the initial porosity $\kappa = S_H n_o$.

Reported hydrate saturations can reach $S_H = 20$–30% in fine-grained sediments ($S_H = 18.2\%$ in the Krishna-Godavari Basin - Yun et al., (2010); $S_H = 19.5\%$ in the Ulleung Basin - Yun et al., (2011)). This would require an initial metabolizable carbon content $\alpha \approx 0.5\%$, an unlikely situation in the field [Paull et al., 1994]. Limited bioactivity in the small pores of fine-grained sediments further aggravates this situation [Phadnis and Santamarina 2011; Rebata-Landa and Santamarina 2006].

In summary, the results from the two previous analyses of hydrate volume fraction formed in closed systems (from solution and from organic matter) imply that some high hydrate concentrations S_H>20% found in the field have involved diffusive and/or advective methane transport.

4. Analyses relevant to gas production

Gas may be produced from hydrate bearing sediments by combinations of depressurization, thermal stimulation or chemical injection. First order analyses are conducted in each case to assess the implications to potential recovery strategies.

4.1. Depressurization: available heat and ice formation

Depressurization is an unlikely production mechanism in fine-grained sediments as the permeability would be reduced due to the increase in effective stress. Yet, depressurization can be used in combination with other methods to develop optimal production strategies.

Hydrate dissociation is highly endothermic (relevant properties are summarized in Table 2). Notably, the energy density required to dissociate methane hydrate $\rho_h L_H$ is equivalent to the energy $\rho_w c_w \Delta T_W$ required to heat water by $\Delta T_{HW} = 96$ °C. For comparison, the energy density required to melt ice $\rho_i L_I$ is equal to the energy required to heat the same mass of water by a temperature change $\Delta T_{IW} = 73$ °C.

Endothermic hydrate dissociation may hinder gas production if secondary ice or hydrate forms along flow paths [Moridis et al., 2011b]. During adiabatic conditions the heat for dissociation must be supplied by the sensible heat within the hydrate-bearing sediment. The initial temperature T_0 and pressure P_0 conditions are inside the hydrate stability field (Fig. 4a). The system *PT* conditions cross the phase boundary at temperature T_T, and reaches the final pressure P_F at a final temperature T_F. The sensible heat E_{HBS} that is available in the volume V_T of the hydrate-bearing sediment is a function of the available heat in the mineral, water, gas, hydrate and the energy produced by ice formation

$$\begin{aligned} E_{HBS} = V_T[&(1-n)\rho_m c_m(T_0 - T_F) + n(1-S_H)\rho_w c_w(T_o - T_F) \\ &+ nS_H\rho_h c_h(T_0 - T_T)] + V_T\left[0.8nS_H\rho_w c_w(T_T - T_F)\right. \\ &\left.+ nS_H\rho_g c_g(T_T - T_F)\right] + V_T[n(1-S_H) + 0.8nS_H]\rho_w L_I FR_{WI} \end{aligned} \tag{11}$$

where n is the porosity of the sediment, and the densities of the mineral, water, hydrate, and gas are ρ_m, ρ_w, ρ_h, and $\rho_g = 16\rho_h/119.5$ [kg/m^3]. Their specific heats are c_m, c_w, c_h, and c_g [kJ/kg·°C]. The term FR_{WI} represents the fraction of the total water converted into ice (the summation of the initial water and the water produced from hydrate dissociation).

However, the energy needed to dissociate hydrate E_{DIS} is a function of the total sediment volume V_T, porosity n, hydrate saturation S_H, hydrate density ρ_h, and the latent heat of hydrate dissociation L_h,

$$E_{DIS} = V_T n S_H \rho_h L_H \tag{12}$$

There is no ice formation when the final temperature of the sediment is above the nominal $T_f = 0$ °C, i.e., there is no heat from ice formation and the third term in Equation (11) is removed. Then, the maximum initial hydrate saturation S_h that does not cause ice formation during adiabatic hydrate dissociation is obtained by setting Equation (11) equal to Equation (12) and $T_f = 0$ °C

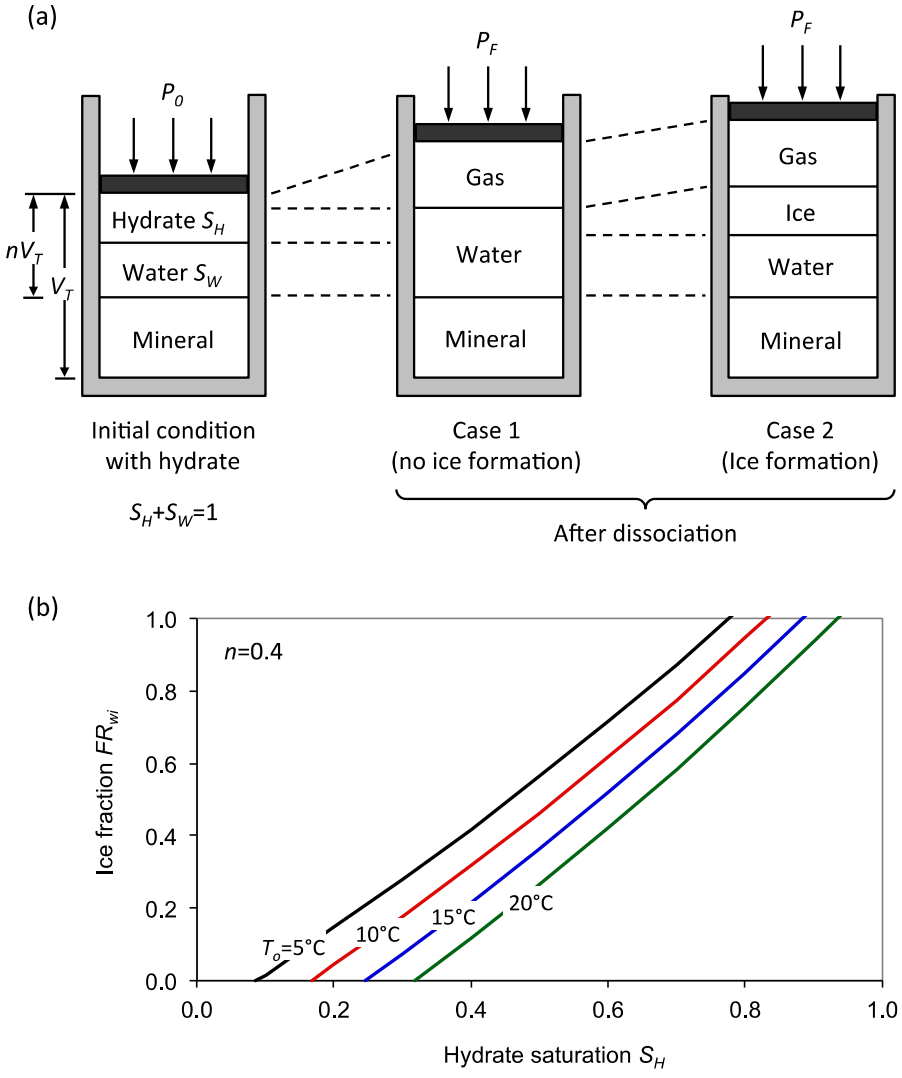

Fig. 4. Hydrate dissociation and subsequent possible ice formation. (a) Hydrate bearing sediment with initial hydrate saturation S_H. Under adiabatic conditions, the energy needed to dissociate hydrate can be supplied by the medium's latent heat (case 1); additional heat may be gained from exothermic ice formation (case 2). (b) Consider hydrate bearing sediments with porosity $n = 0.4$ at initial temperatures $T_o = 5$, 10, 15, and 20 °C depressurized to $P_{eq} = 3$ MPa so that the hydrate equilibrium temperature is $T_{eq} = 2.5$ °C. Ice does not form if initial hydrate saturation is $S_H = 0.09$, 0.17, 0.25, and 0.32 for each initial temperature conditions. As the initial hydrate saturation increases, the amount of ice formed due to hydrate dissociation also increases. Ice fraction FR_{wi} is the portion of water (initial water and water from hydrate dissociation) converted into ice. Values of specific heat for minerals, water, gas, and hydrate and of latent heat of hydrate dissociation and ice formation are listed in Table 2.

$$S_H = \frac{(1-n)\alpha_m T_0 + nT_0}{n\beta_h + nT_0 - n\alpha_h(T_0 - T_T) - 0.8nT_T - n\alpha_g T_T} \quad (T_o \text{ and } T_t \text{ in}^\circ C) \tag{13}$$

where the density times the specific heat of species ρc is normalized by the corresponding value for water $\rho_w c_w$, so that $\alpha_m = \rho_m c_m/\rho_w c_w$, $\alpha_h = \rho_h c_h/\rho_w c_w$, and $\alpha_g = \rho_g c_g/\rho_w c_w$. The same normalization is enforced for the product of the hydrate density and the latent heat of dissociation $\beta_h = \rho_h L_H/\rho_w c_w$. For example, Equation (13) anticipates that ice would not form when the initial hydrate saturation is $S_H = 9\%$ in a reservoir at the initial temperature $T_0 = 5$ °C, $S_H = 17\%$ when $T_0 = 10$ °C, $S_H = 25\%$ when $T_0 = 15$ °C, or $S_H = 32\%$ when $T_0 = 20$ °C. These results correspond to a sediment porosity $n = 0.4$ and transformation temperature $T_T = 2.5$ °C; other parameters are in Table 2.

The fraction of ice FR_{wi} formed during hydrate dissociation when the hydrate saturation exceeds values predicted by Equation (13) is obtained by combining Equations (11) and (12):

$$FR_{WI} = \frac{nS_H\beta_h - (1-n)\alpha_m(T_0 - T_F) - n(1-S_H)(T_0 - T_F) - nS_H\alpha_h(T_0 - T_T) - 0.8nS_H(T_T - T_F) - nS_H\alpha_g(T_T - T_F)}{[n(1-S_H) + 0.8nS_H]\beta_I} \tag{14}$$

where β_I is the ratio of the heat of transformation of water to the specific heat of water $\beta_I = L_I/c_w$.

Fig. 4b shows the fraction FR_{WI} of the total water converted into ice as a function of hydrate saturation S_H for reservoirs at different initial temperatures T_0. All the water freezes when the initial hydrate saturation is $S_H \approx 0.78$ in a reservoir with initial temperature $T_0 = 5$ °C. These results highlight the advantages of deeper and warmer reservoirs, and are in agreement with observations based on complex reservoir simulators [Anderson et al., 2011; Moridis et al., 2011a].

4.2. Heating: volume change

The volume of hydrate V_H expands into a significantly larger volume of water and gas $V_W + V_G$ upon dissociation for *PT* conditions that are relevant to the marine hydrate accumulations currently under consideration. A simple expression for the fluid expansion $\eta=(V_G + V_W)/V_H$ is calculated using a modified ideal gas law $PV = \omega nRT$

$$\begin{aligned}\eta &= \frac{V_G + V_W}{V_h} \\ &= \frac{\omega\lambda RT}{P} + \frac{18\chi}{16+18\chi}\frac{\rho_h}{\rho_w} \\ &= \frac{\omega\lambda RT}{P} + \frac{18\chi}{16+18\chi}\frac{\rho_h}{\rho_w} \\ &\approx 0.057\left[\frac{\text{MPa}}{\text{K}}\right]\frac{T}{P} + 0.79\end{aligned} \tag{15}$$

The last approximation is obtained by setting the "compressibility factor" $\omega \approx 0.95$ to adjust the ideal gas law to the *Peng-Robinson* equation within the *P-T* range of interest, the amount of methane per unit volume of hydrate $\lambda \approx 7.37 \times 10^3$ mol/m^3, the hydration number $\chi \approx 6$, the universal gas constant $R = 8.314$ J/(mol K), and the mass density ratio $\rho_h/\rho_w \approx 0.91$ For example, the volume of hydrate will expand $\eta = 4.0$ times just to cross the phase boundary during dissociation for $P_W = 5$ MPa and $T_T = 279.4$ K; similarly, the expansion will be $\eta = 2.4$ times for $P_W = 10$ MPa and $T_T = 285.6$ K. Clearly, further depressurization away from the phase boundary will lead to additional gas expansion. Note: capillary pressure is not taken into consideration because we assume that gas produced from segregated hydrate will be found in relatively large open pores and discontinuities.

Fluid attempts to expand during dissociation; at the same time the small pores in clayey sediments hinder gas expansion. Consequently, widespread gas-driven fractures will develop in hydrate bearing clayey sediments during thermally driven dissociation (underlying mechanisms are analyzed in Shin and Santamarina (2011)).

4.3. CO_2–CH_4 replacement: thermal and volumetric changes

The volume hydrate occupies V_H is larger than the volume of water consumed V_w both for CH_4 hydrate ($V_{CH4\text{-}H}/V_W \approx 1.23$) and for CO_2 hydrate ($V_{CO2\text{-}H}/V_W \approx 1.28$). It follows that a relatively minor hydrate volume expansion will take place during complete CO_2–CH_4 replacement: $V_{CO2\text{-}H}/V_{CH4\text{-}H} = 1.28/1.23 = 1.04$ [Jung et al., 2010]).

Given the latent heats for CH_4 $L_H = 440$ kJ/kg and CO_2 hydrate $L_H = 374$ kJ/kg and densities for CH_4 hydrate $\rho_{CH4} = \sim 0.91$ g/cm^3 and CO_2 hydrate $\rho_{CO2} = \sim 1.10$ g/cm^3, the CH_4–CO_2 replacement is exothermic (Table 2). The thermal analysis of CH_4–CO_2 replacement under adiabatic conditions demonstrates that the sediment temperature will increase by 0.2 °C when the hydrate volume fraction is $S_H = 0.2$ and the sediment porosity is $n = 0.4$, Note: the local thermal transient at the point of exchange can exceed $\Delta T \sim 10$ °C [Jung et al., 2010].

The volume of liquid CO_2 $V_{CO2\text{-}L}$ required to fully replace CH_4 can be estimated by assuming complete replacement for a volume $V_{CH4\text{-}H}$ of methane hydrate:

$$\frac{V_{CO2-L}}{V_{CH4-H}} = \frac{\rho_{CH4-H}}{\rho_{CO2-L}}\frac{44}{16+\chi 18} \approx 0.34 \tag{16}$$

The approximation on the right assumes the hydration number $\chi = 6$ and the density ratio between CH_4 hydrate and liquid CO_2 to be $\rho_{CH4\text{-}H}/\rho_{CO2\text{-}L} = 0.97$ (at $P = 10$ MPa and $T = 7$ °C - Table 2).

The released CH_4 is a compressible gas and will occupy a volume $V_{CH4\text{-}G}$ that can be significantly larger than the volume $V_{CO2\text{-}L}$ of injected liquid CO_2. The volumetric ratio is estimated from the modified ideal gas law with the following assumptions: no mutual solubilities, no fluid extraction from the sediment and complete replacement,

$$\begin{aligned}\frac{V_{CH4-G}}{V_{CO2-L}} &= \frac{\omega n_{CH4-H}RT}{P}\frac{1}{V_{CO2-L}} \\ &= \frac{\omega RT}{P}\frac{1}{V_{CO2-L}}\rho_{CH4-H}V_{CH4-H}\frac{1}{16+\chi 18} \\ &= \frac{\omega RT}{P}\rho_{CO2-L}\frac{16+\chi 18}{44}\frac{1}{16+\chi 18} \\ &\approx 0.168\left[\frac{\text{MPa}}{\text{K}}\right]\frac{T}{P}\end{aligned} \tag{17}$$

where $n_{CH4\text{-}H}$ is the mole of methane in CH_4 hydrate. We obtain the final simplified expression for a compressibility factor $\omega = 0.95$, hydration number $\chi = 6$, and liquid CO_2 density $\rho_{CO2\text{-}L} = 938$ kg/m^3. We anticipate a large volume expansion under constant pressure conditions, e.g., $V_{CH4\text{-}G}/V_{CO2\text{-}L} \approx 4.7$ at 10 MPa and 280 K. Conversely, high fluid pressure builds up if a constant-volume is imposed, e.g., about 34.7 MPa at 7 °C. This upper bound estimate assumes all components are incompressible and disregards mutual solubilities. In fact, the most significant solubility is that of water in liquid CO_2, in the order of 0.063 mol/kg, i.e., 1.13 g of water per 1 kg of liquid CO_2, at 8.3 MPa and 287 K [Song and Kobayashi 1987].

Implications. During CH_4–CO_2 replacement, a shell of CO_2 hydrates forms around existing CH_4 hydrates, which reduces the kinetics of the replacement process [Schicks et al., 2011]. The liberated CH_4 molecules remain in pore spaces, which further reduces the driving force for the replacement process. While CO_2–CH_4 replacement presents these implementation challenges in the field, the analyses in this section provide two favorable conditions. Firstly, the heat released during CO_2–CH_4 replacement will sustain the reaction. Secondly, the volume expansion will maintain open lenses, prevent conductivity shut-off, and even create new open mode discontinuities that will favor gas recovery.

5. Discussion: relevance to other sediments

Pore size is determined by the smallest grains in a sediment. Let's define the mass fraction of fine particles φ as the ratio between the mass of fines M_F to the total mineral mass of the sediment M_T. It can then be demonstrated that the mass fraction of fine particles needed to fill the pores in a sandy sediment depends on the packing density or void ratio e_f of the fines within the pore space of the sand matrix packed at a void ratio e_c:

$$\varphi = \frac{M_F}{M_T} = \frac{e_c}{1+e_c+e_f} \quad \text{fines fraction} \tag{18}$$

The lower bound for φ corresponds to loosely packed fines within the pore space of a densely packed sand. Consider the case of fines packed at a void that corresponds to their liquid limit and sand at a void ratio $e_c = 0.7$. Then, Equation (18) predicts that the fines fraction is $\varphi = 30\%$ when the sand is filled with a non-plastic silt (LL = 25, $e_f = 0.66$), $\varphi = 23\%$ for kaolinite (LL = 55, $e_f = 1.45$), and only $\varphi = 7\%$ when voids in the sand are filled with montmorillonite (LL = 300, $e_f = 7.95$). Therefore, special attention should be placed on the amount and mineralogy of fines within a sediment.

Fluid flow often introduces fine particles into otherwise clean sands and leads to clogging and gas-driven fractures during production [Jung et al., 2012]. Grains also crush and produce fines within the formation when there is a high increase in effective stress, such as near wells in depressurization-driven gas production.

The analyses of secondary ice formation during depressurization (Equations (11)–(14)), volume expansion in thermal stimulation (Equation (15)), and thermal changes and expansion during CO_2–CH_4 replacement (Equations (16) and (17)) are applicable to all sediments.

6. Conclusions

Hydro-thermo-chemo-mechanical coupled processes during hydrate formation and dissociation affect hydrate morphology in sediments and control gas production during depressurization, heating and CO_2–CH_4 replacement. Balance and conservation analyses anchored in published data provide robust asymptotic solutions that reflect a number of governing processes. Salient observations from this study are organized into three categories.

Relevant sediment characteristics:

- Specific surface and porosity define pore size. In turn, the pore size determines permeability and capillarity, and also affects the phase boundary when pores are <100 nm.
- Pore size is determined by the smallest grains in a sediment. Even a small amount of fine particles can fill the pore space in sands. Therefore the characterization of sandy deposits must carefully consider the amount and mineralogy of clayey fines.
- Particle size (i.e., specific surface), effective stress and capillarity regulate the potential for hydrate segregation. In agreement with field evidence, hydrate lenses and nodules are anticipated in clayey sediments.
- A hydrate bearing clayey sediment is a two-material system where segregated hydrate is surrounded by hydrate-free water saturated clay.

Hydrate formation:

- The excess dissolved gas in the pore water can concentrate to form $S_H \approx 2\%$ hydrate saturation. Furthermore, a hydrate saturation of $S_H \approx 20\%$ could develop in fine-grained sediments if the initial metabolizable carbon content was as high as ≈0.5%.
- Higher hydrate saturations that are often found in-situ in the form of lenses and nodules imply that additional methane was transported by advection and/or diffusion.

Gas production:

- Hydrate dissociation is strongly endothermic. The energy density required to dissociate methane hydrate is equivalent to the energy required to cause a 96 °C increase in the temperature of the same mass of water. In the extreme case of adiabatic conditions, the available latent heat in a reservoir at an initial temperature of 10 °C is sufficient to sustain the dissociation of $S_H = 17\%$ without triggering ice formation during depressurization. However, all the available water will freeze when the initial hydrate saturation is $S_H \approx 80\%$. Ice or secondary hydrate formation hinders gas production if it accumulates along flow paths.
- Depressurization is an unlikely production mechanism in fine-grained sediments as the permeability would tend to decrease significantly. Yet, depressurization can be used in combination with other methods such as heating and chemical injection to develop optimal production strategies.
- The volume that hydrate occupies expands into a significantly larger volume of water and gas during dissociation. Expansion factors can vary between 2 and 4 for field conditions of interest. Widespread gas-driven fractures are anticipated upon volume expansion in fine grained sediments.
- The phase boundary for methane mixed with carbon dioxide shifts with the mixture ratio. Methane hydrate bearing sediments are typically encountered under PT conditions such that injected CO_2 will be in liquid phase and will tend to form CO_2 hydrate with free water. The heat released during CO_2–CH_4 replacement sustains the reaction. The volume of released methane is ~5 times larger than the volume of injected liquid CO_2 under common reservoir conditions. Volume expansion will maintain lenses open and create new open mode discontinuities that will favor methane gas recovery.

Acknowledgements

Support for this research was provided by DOE/NETL Methane Hydrate Project (DE-FC26-06NT42963). Additional support was provided by the Goizueta Foundation and KAUST's endowment.

References

Adisasmito, S., Frank, R.J., Sloan, E.D., 1991. Hydrates of carbon dioxide and methane mixtures. J. Chem. Eng. Data 36 (68–71).

Anderson, B.J., et al., 2011. Regional long-term production modeling from a single well test, mount elbert gas hydrate stratigraphic test well, Alaska north slope. Mar. Petroleum Geol. 28 (2), 493–501. http://dx.doi.org/10.1016/j.marpetgeo.2010.01.015.

Anderson, G.K., 2003. Enthalpy of dissociation and hydrate number of carbon dioxide from the Clapeyron equation. J. Chem. Thermodyn. 35, 1171–1183.

Anderson, R., Llamedo, M., Tohidi, B., Burgass, R.W., 2003. Experimental measurement of methane and carbon dioxide clathrate hydrate equilibria in mesoporous silica. J. Phys. Chem. B 107 (15), 3507–3514. http://dx.doi.org/10.1021/jp0263370.

Aya, I., Yamane, K., Nariai, H., 1997. Solubility of CO_2 and density of CO_2 hydrate at 30MPa. Energy 22, 263–271.

Bhatnagar, G., Chapman, W.G., Dickens, G.R., Dugan, B., Hirasaki, G.J., 2007. Generalization of gas hydrate distribution and saturation in marine sediments by scaling of thermodynamic and transport processes. Am. J. Sci. 307 (6), 861–900. http://dx.doi.org/10.2475/06.2007.01.

Boswell, R., 2009. Is gas hydrate energy within reach? Science 325, 957–958.

Boswell, R., Collett, T.S., 2011. Current perspectives on gas hydrate resources. Energy & Environ. Sci. 4 (4), 1206. http://dx.doi.org/10.1039/c0ee00203h.

Burland, J.B., 1990. On the compressibility and shear strength of natural clays. Geotechnique 40 (3), 329–378.

Circone, S., Stern, L.A., Kirby, S.H., Durham, W.B., Chakoumakos, B.C., Rawn, C.J., Rondinone, A.J., Ishii, Y., 2003. CO2 hydrate: synthesis, composition, structure, dissociation behavior, and a comparison to structure I CH4 hydrate. J. Phys. Chem. B 107, 5529–5539.

Clennell, M.B., Hovland, M., Booth, J.S., Henry, P., Winters, W.J., 1999. Formation of natural gas hydrates in marine sediments 1. Conceptual model of gas hydrate growth conditioned by host sediment properties. J. Geophys. Res. 104 (B10), 22985–23003.

Dai, S., Lee, C., Carlos Santamarina, J., 2011. Formation history and physical properties of sediments from the mount elbert gas hydrate stratigraphic test well, Alaska north slope. Mar. Petroleum Geol. 28 (2), 427–438. http://dx.doi.org/10.1016/j.marpetgeo.2010.03.005.

Dai, S., Santamarina, J.C., Waite, W.F., Kneafsey, T.J., 2012. Hydrate morphology: physical properties of sands with patchy hydrate saturation. J. Geophys. Res. 117 (B11205) http://dx.doi.org/10.1029/2012jb009667.

Davie, M.K., Buffett, B.A., 2001. A numerical model for the formation of gas hydrate below the seafloor. J. Geophys. Res. 106 (B1), 497. http://dx.doi.org/10.1029/

2000jb900363.
Davie, M.K., Zatsepina, O.Y., Buffett, B.A., 2004. Methane solubility in marine hydrate environments. Mar. Geol. 203 (1–2), 177–184. http://dx.doi.org/10.1016/s0025-3227(03)00331-1.
Dickens, G.R., Quinby-Hunt, M.S., 1997. Methane hydrate stability in pore water: a simple theoretical approach for geophysical applications. J. Geophys. Res. 102 (B1), 773–783.
Donnelly, H.G., Katz, D.L., 1954. Phase equilibria in the carbon dioxide–methane system. Industrial Eng. Chem. 46 (3), 511–517. http://dx.doi.org/10.1021/ie50531a036.
Duan, Z., Sun, R., 2003. An improved model calculating CO2 solubility in pure water and aqueous NaCl solutions from 273 to 533 K and from 0 to 2000 bar. Chem. Geol. 193, 257–271.
Duan, Z., Mao, S., 2006. A thermodynamic model for calculating methane solubility, density and gas phase composition of methane-bearing aqueous fluids from 273 to 523K and from 1 to 2000bar. Geochimica Cosmochimica Acta 70 (13), 3369–3386. http://dx.doi.org/10.1016/j.gca.2006.03.018.
Dvorkin, J., Helgerud, M.B., Waite, W.F., Kirby, S.H., Nur, A., 2000. Introduction to physical properties and elasticity models. In: Max, M.D. (Ed.), Natural Gas Hydrate: in Oceanic and Permafrost Environments. Kluwer Acad, Dordrecht, Netherlands, pp. 245–260.
Engineering ToolBox (Material properties, available at http://www.engineeringtoolbox.com).
Espinoza, D.N., Santamarina, J.C., 2010. Water-CO_2-mineral systems: interfacial tension, contact angle and diffusion–Implications to CO_2 geological storage. Water Resour. Res. 46, W07537. http://dx.doi.org/10.1029/2009WR008634.
Folas, G.K., Froyna, E.W., Lovland, J., Kontogeorgis, G.M., Solbraa, E., 2007. Data and prediction of water content of high pressure nitrogen, methane and natural gas. Fluid Phase Equilibria 252 (1–2), 162–174. http://dx.doi.org/10.1016/j.fluid.2006.12.018.
Handa, Y.P., Stupin, D., 1992. Thermodynamic properties and dissociation characteristics of methane and propane hydrates in 70-Å-radius silica gel pores. J. Phys. Chem. 96, 8599–8603.
Handa, Y.P., Hawkins, R.E., Murray, J.J., 1984. Calibration and testing of a Tian-Calvet heat-flow calorimeter enthalpies of fusion and heat capacities for ice and tetrahydrofuran hydrate in the range 85 to 270K. J. Chem. Thermodyn. 16, 623–632.
Handa, Y.P., 1986. Compositions, enthalpies of dissociation, and heat capacities in the range 85 to 270 K for clathrate hydrates of methane, ethane, and propane, and enthalpy of dissociation of isobutene hydrates, as determined by a heat-flow calorimeter. J. Chem. Thermodyn. 18, 915–921.
Hashemi, S., Macchi, A., Bergeron, S., Servio, P., 2006. Prediction of methane and carbon dioxide solubility in water in the presence of hydrate. Fluid Phase Equilibria 246 (1–2), 131–136. http://dx.doi.org/10.1016/j.fluid.2006.05.010.
Helgerud, M.B., Waite, W.F., Kirby, S.H., Nur, A., 2009. Elastic wave speeds and moduli in polycrystalline ice Ih, sI methane hydrate, and sII methane-ethane hydrate. J. Geophys. Res. 114, B02212.
Henry, P., Thomas, M., Clennell, M.B., 1999. Formation of natural gas hydrates in marine sediments: 2. Thermodynamic calculations of stability conditions in porous sediments. J. Geophys. Res. 104 (B10), 23005. http://dx.doi.org/10.1029/1999jb900167.
Jung, J.W., Espinoza, D.N., Santamarina, J.C., 2010. Properties and phenomena relevant to CH4-CO2replacement in hydrate-bearing sediments. J. Geophys. Res. 115 (B10) http://dx.doi.org/10.1029/2009jb000812.
Jung, J.W., Jang, J., Santamarina, J.C., Tsouris, C., Phelps, T.J., Rawn, C.J., 2012. Gas production from hydrate-bearing sediments: the role of fine particles. Energy Fuels 26, 480–487. http://dx.doi.org/10.1021/ef101651b.
Kang, S.P., Lee, H., Rhy, B.J., 2001. Enthalpies of dissociation of clathrate hydrates of carbon dioxide, nitrogen, (carbon dioxide + nitrogen), and (carbon dioxide + nitrogen + tetrhydrofuran). J. Chem. thermidynamics 33, 513–521.
Kaye, G.W.C., Laby, T.H., 2007. Tables of Physical and Chemical Constants, sixteenth ed. National Physical Laboratory, Middlesex, U.K. available at: www.kayelaby.npl.co.uk.
Kiefte, H., Clouter, M.J., Gagnon, R.E., 1985. Determination of acoustic velocities of clathrate hydrates by brillouin spectroscopy. J. Phys. Chem. 89, 3103–3108.
Klapproth, A., Goreshnik, E., Staykova, D., Klein, H., Kuhs, W.F., 2003. Structural studies of gas hydrates. Can. J. Phys. 81 (1–2), 503–518. http://dx.doi.org/10.1139/p03-024.
Kwon, T.-H., Cho, G.-C., Santamarina, J.C., 2008. Gas hydrate dissociation in sediments: pressure-temperature evolution. Geochem. Geophys. Geosystems 9 (3). http://dx.doi.org/10.1029/2007gc001920 n/a-n/a.
Leaist, D.G., Murray, J.J., Post, M.L., Davidson, D.W., 1982. Enthalpies of decomposition and heat capacities of ethylene oxide and tetrahydrofuran hydrates. J. Phys. Chem. 86, 4175–4178.
Lievois, J.S., Perkins, R., Martin, R.J., Kobayashi, R., 1990. Development of an automated, high pressure heat flux calorimeter and its application to measure the heat of dissociation and hydrate numbers of methane hydrate. Fluid phase equilibria 59, 73–97.
Lu, W., Chou, I.M., Burruss, R.C., 2008. Determination of methane concentrations in water in equilibrium with sI methane hydrate in the absence of a vapor phase by in situ Raman spectroscopy. Geochimica Cosmochimica Acta 72 (2), 412–422. http://dx.doi.org/10.1016/j.gca.2007.11.006.
Malinverno, A., 2010. Marine gas hydrates in thin sand layers that soak up microbial methane. Earth Planet. Sci. Lett. 292 (3–4), 399–408. http://dx.doi.org/10.1016/j.epsl.2010.02.008.
Moridis, G.J., Silpngarmlert, S., Reagan, M.T., Collett, T., Zhang, K., 2011a. Gas production from a cold, stratigraphically-bounded gas hydrate deposit at the mount elbert gas hydrate stratigraphic test well, Alaska north slope: implications of uncertainties. Mar. Petroleum Geol. 28 (2), 517–534. http://dx.doi.org/10.1016/j.marpetgeo.2010.01.005.
Moridis, G.J., et al., 2011b. Challenges, uncertainties, and issues facing gas production from gas-hydrate deposits. SPE Reserv. Eval. Eng. 14 (1), 76–112.
Osegovic, J.P., Tatro, S.R., Holman, S.A., 2006. Chapter 2. Physical chemical characteritics of natural gas hydrate. In: Max, M.D., Johnson, A.H., Dillon, W.P. (Eds.), Economic Geology of Natural Gas Hydrate. Springer, Dordrecht, The Netherlands.
Paull, C.K., Ussler, W., Borowski, W.S., 1994. Sources of biogenic methane to form marine gas hydrates. In: Sloan, E.D., Happel, J., Hnatow, M.A. (Eds.), Natural Gas Hydrates. Annals New York Academy of Sciences, pp. 392–409.
Phadnis, H.S., Santamarina, J.C., 2011. Bacteria in sediments: pore size effects. Géotechnique Lett. 1, 91–93. http://dx.doi.org/10.1680/geolett.11.00008. October-December.
Qin, J., Rosenbauer, R.J., Duan, Z., 2008. Experimental measurments of vapor-liquid equilibria of the H2O+CO2 +CH4 ternary system. J. Chem. Eng. Data 53, 1246–1249.
Rebata-Landa, V., Santamarina, J.C., 2006. Mechanical limits to microbial activity in deep sediments. Geochem. Geophys. Geosystems 7 (11), Q11006.
Ren, Q.-Y., Chen, G.-J., Yan, W., Guo, T.-M., 2000. Interfacial tension of (CO_2+CH_4)+ water from 298K to 373K and pressures up to 30MPa. J. Chem. Eng. data 45, 610–612.
Rueff, R.M., Sloan, E.D., Yesavage, V.F., 1988. Heat capacity and heat of dissociation of methane hydrates. AIChE J. 34 (9), 1468–1476.
Santamarina, J.C., Jang, J., 2010. Energy geotechnology: implications of mixed fluid conditions. In: Paper Presented at 5th International Conference on Unsaturated Soils, Bacelona, Spain.
Schicks, J.M., Luzi, M., Beeskow-Strauch, B., 2011. The conversion process of hydrocarbon hydrates into CO2 hydrates and vice versa: thermodynamic considerations. J. Phys. Chem. A 115 (46), 13324–13331. http://dx.doi.org/10.1021/jp109812v.
Seo, Y., Lee, H., Uchida, T., 2002. Methane and carbon dioxide hydrate phase behavior in small porous silica gels: three-phase equilibrium determination and thermodynamic modeling. Langmuir 18, 9164–9170.
Servio, P., Englezos, P., 2001. Effect of temperature and pressure on the solubility of carbon dioxide in water in the presence of gas hydrate. Fluid Phase Equilibria 190, 127–134.
Servio, P., Englezos, P., 2002. Measurement of dissolved methane in water in equilibrium with its hydrate. J. Chem. Eng. Data 47, 87–90.
Shin, H., Santamarina, J.C., 2011. Open-mode discontinuities in soils. Géotechnique Lett. 1, 95–99. http://dx.doi.org/10.1680/geolett.11.00014. October-December.
Skempton, A.W., 1969. The consolidation of clays by gravitational compaction. Q. J. Geol. Socienty Lond. 125, 373–411.
Sloan, E.D., Koh, C.A., 2008. Clathrate Hydrates of Natural Gases, third ed. CRC Press, Taylor & Francis Group, Boca Raton, FL.
Smith, D.H., Wilder, J.W., Seshadri, K., 2002a. Methane hydrate equilibria in silica gels with broad pore-size distributions. AIChE J. 48 (2), 393–400.
Smith, D.H., Wilder, J.W., Seshadri, K., 2002b. Thermodynamics of carbon dioxide hydrate formation in media with broad pore-size distributions. Environ. Sci. Technol. 36, 5192–5198.
Song, K.Y., Kobayashi, R., 1987. Water content of CO2 in equilibrium with liquid water and/or hydrates. SPE Form. Eval. 2 (4), 500–508.
Span, R., Wagner, W., 1996. A new equation of state for carbon dioxide covering the fluid region from the triple-point temperature to 1100K at pressures up to 800MPa. J. Phys. Chem. reference data 25 (6), 1509–1596.
Sun, R., Duan, Z., 2005. Prediction of CH4 and CO2 hydrate phase equilibrium and cage occupancy from ab initio intermolecular potentials. Geochimica Cosmochimica Acta 69 (18), 4411–4424. http://dx.doi.org/10.1016/j.gca.2005.05.012.
Sun, R., Duan, Z., 2007. An accurate model to predict the thermodynamic stability of methane hydrate and methane solubility in marine environments. Chem. Geol. 244 (1–2), 248–262. http://dx.doi.org/10.1016/j.chemgeo.2007.06.021.
Sychev, V.V., Vasserman, A.A., Zagoruchenko, V.A., Spiridonov, G.A., Tsymarny, V.A., 1987. Thermodynamic Properties of Methane, p. 341 (Hemisphere, Washington, D.C).
Terzaghi, K., Peck, R.B., 1948. Soil Mechanics in Engineering Practice. John Wiley, New York.
Tishchenko, P., Hensen, C., Wallmann, K., Wong, C.S., 2005. Calculation of the stability and solubility of methane hydrate in seawater. Chem. Geol. 219 (1–4), 37–52. http://dx.doi.org/10.1016/j.chemgeo.2005.02.008.
Uchida, T., Ebinuma, T., Ishizaki, T., 1999. Dissociation condition measurements of methane hydrate in confined small pores of porous glass. J. Phys. Chem. B 103, 3659–3662.
Uchida, T., Ebinuma, T., Takeya, s., Nagao, J., Narita, H., 2002. Effects of pore sizes on dissociation temperatures and pressures of methane, carbon dioxide, and propane hydrates in porous media. J. Phys. Chem. B 106, 820–826.
Waite, W.F., et al., 2009. Physical properties of hydrate-bearing sediments. Rev. Geophys. 47 (4).
Weast, R.C., 1987. CRC Handbook of Chemistry and Physics, 68ed. CRC Press, Boca

Raton, Fla.
Wilhelm, E., Battino, R., Wilcock, R.J., 1977. Low-pressure solubility of gases in liquid water. Chem. Rev. 77 (2), 219–262.
Yun, T.S., Fratta, D., Santamarina, J.C., 2010. Hydrate-bearing sediments from the Krishna–Godavari basin: physical characterization, pressure core testing, and scaled production monitoring. Energy Fuels 24 (11), 5972–5983. http://dx.doi.org/10.1021/ef100821t.
Yun, T.S., Lee, C., Lee, J.-S., Bahk, J.J., Santamarina, J.C., 2011. A pressure core based characterization of hydrate-bearing sediments in the Ulleung Basin, Sea of Japan (East Sea). J. Geophys. Res. 116 (B2) http://dx.doi.org/10.1029/2010jb007468.
Zatsepina, O.Y., Buffett, B.A., 1998. Thermodynamic conditions for the stability of gas hydrate in the seafloor. J. Geophys. Res. 103 (B10), 24127–24139.